Non-Hermitian time evolution: From static to parametric instability

Aleksi Bossart [*] and Romain Fleury [†]

Laboratory of Wave Engineering, Ecole Polytechnique Fédérale de Lausanne, 1015 Lausanne, Switzerland

Eigenmode coalescence imparts remarkable properties to non-Hermitian time evolution, culminating in a purely non-Hermitian spectral degeneracy known as an exceptional point (EP). Here, we revisit time evolution around EPs, looking at both static and periodically modulated non-Hermitian Hamiltonians. We connect a Möbius group classification of two-level non-Hermitian Hamiltonians with the theory of Hill's equation, which unlocks a large class of analytical solutions. Together with the classification, this allows us to investigate the impact of the shape of the temporal modulation on the long-term dynamics of the system. In particular, we find that EP encircling does not predict the temporal class, and that the elaborate interplay between non-Hermitian and modulation instabilities is better understood through the lens of parametric resonance. Finally, we identify specific signatures of complex parametric resonance by exhibiting stability diagrams with features that cannot occur in traditional parametric resonance.

I. INTRODUCTION

Non-Hermitian Hamiltonians model nonconservative systems, such as paraxial waveguides or coupled resonators with gain and loss [1]. Such traditional non-Hermitian systems are usually time invariant and exhibit standard instabilities originating from gain of static nature. More interestingly, the absence of a spectral theorem for these Hamiltonians gives rise to unconventional behavior. The most striking example is a type of purely non-Hermitian spectral degeneracy in which the eigenvectors collapse as well: the so-called exceptional point (EP) [1–7]. These degeneracies have a long history, dating back to studies of nondiagonalisable dielectric tensors by Pancharatnam [2] and mathematical studies of linear operators [3] with a turning point marked by the advent of pseudo-Hermitian quantum theory [8–10]. Both theoretical and experimental studies have proposed EPs for superior sensors [11–14], whereas recent theoretical studies started delineating the limitations of such EP-based sensing [15,16]. Another promising application is that of EP-based polarizers, which have been explored in several studies [17–21].

Lifting an EP degeneracy defines a *Riemann surface*, namely, a complex manifold that locally looks like the complex plane but may have a different topology [22]. In order to explore EP properties associated with these surfaces, a fruitful strategy consists of varying the Hamiltonian's parameters in time in order to encircle the EP, a feat known as *dynamical EP encircling* [17,23–25]. This process has been theorized to give rise to chiral mode conversion and has since been realized in many experimental settings [17,19,26–28]. In adiabatic EP encircling, the behavior of the system is well understood with respect to the properties of the instantaneous Hamiltonian over the modulation trajectory. This is, however, not the case for general nonadiabatic periodic modulations, which unleash a whole new class of Floquet non-Hermitian systems [29–38] that may exhibit gain of parametric nature [33,35,36,38]. Deviations from the adiabatic theorem have been studied in the case of particular modulation schemes, mostly circular trajectories [18,39,40], but also modulations involving multiple frequency components [41]; however, the role of EP encircling and the importance of the modulation details (speed, strength, and center) is not well understood. A general theory of static and Floquet non-Hermitian time evolution is still missing and crucial to understand the interplay between the static non-Hermitian properties of the unmodulated system and periodic dynamic modulation.

In this paper, we extend a classification of non-Hermitian time evolution [42] to larger Hilbert spaces and time-modulated Hamiltonians. Equipped with this tool, we unveil the relationship between non-Hermitian and parametric instabilities, including the role of EP encircling. In the first section, we focus on time-independent non-Hermitian systems and explain how time evolution works in the absence of a full set of eigenmodes (i.e., at the EP). To see how this relates to the situation at neighboring points, we present a classification of 2×2 non-Hermitian Hamiltonians based on the Möbius group, previously introduced in Ref. [42], which characterizes the dynamics of the state's polarization, regardless of underlying symmetries. We then extend this Möbius group picture to higher-order Hamiltonians, using a generalization of hyperbolic functions. In the second part of the paper, we introduce a map from periodically modulated Hamiltonians to a Hill differential equation [43], which yields exact solutions that we can also interpret in terms of the Möbius group. On the basis of these solutions, we gain insight on the long-time dynamics of Floquet systems: We provide examples of various Möbius classes in this time-modulated setting and probe their dependency on the modulation parameters. As a

---

[*]aleksi.bossart@epfl.ch

[†]romain.fleury@epfl.ch

by-product, we also demonstrate that Floquet EPs can arise for time modulations that are neither close to nor encircle the static EP. Then, we unveil the origin of the different Floquet non-Hermitian classes by connecting them to the phenomenon of parametric resonance. Finally, our explicit connection to Hill's equation allows us to precisely qualify some of the exotic stability properties that can only arise at the intersection of non-Hermiticity and temporal modulation.

II. NON-HERMITIAN DYNAMICS WITH CONSTANT HAMILTONIANS

In this section, we discuss the time evolution at an EP and present a classification of 2×2 non-Hermitian Hamiltonians, which was previously introduced in Ref. [42] in the context of classical spin dynamics. We then extend this interpretation to higher-order Hamiltonians. Let us begin with a short reminder of time evolution in Hermitian quantum mechanics to bring contrast with the non-Hermitian situation. In the Hermitian case, the Schröödinger equation,

$$i\hbar \frac{\partial}{\partial t} |\psi(t)\rangle = (\hat{h}) |\psi(t)\rangle \tag{1}$$

can, in principle, be solved by putting the Hamiltonian $(\hat{h})$ in diagonal form, thus, effectively decoupling the evolution of all eigenstates $|\boldsymbol{\phi}_k\rangle$. They all follow a simple oscillating time evolution,

$$|\boldsymbol{\phi}_k(t)\rangle = e^{(iE_k/\hbar)t} |\boldsymbol{\phi}_k(0)\rangle. \tag{2}$$

The time evolution for arbitrary states is, thus, easily determined by expressing them in the eigenstate basis of H and then evolving each component according to Eq. (2). This is always possible in principle since the spectral theorem guarantees that Hermitian matrices are diagonalizable. In the following, we lift this Hermiticity restriction and derive the consequences for time evolution, starting with the extreme case of an EP.

A. Exceptional points

We consider a general 2×2 Hamiltonian,

$$H := \begin{pmatrix} a & b \\ c & d \end{pmatrix}, \tag{3}$$

with unrestricted complex entries. Since we are interested in EPs, let us see when the eigenvalues coalesce. To this end, we compute the characteristic polynomial and complete the square,

$$\begin{aligned} \chi(\lambda) &= (a - \lambda)(d - \lambda) - bc \\ &= \left(\lambda - \frac{a+d}{2}\right)^2 + ad - bc - \frac{(a+d)^2}{4}. \end{aligned} \tag{4}$$

Introducing the variables $\tau = \frac{a+d}{2}$ and $\eta = \frac{a-d}{2}$, we get the following condition for eigenvalue collapse:

$$bc = -\eta^2. \tag{5}$$

Eigenvalue collapse is a necessary but insufficient condition for EPs to occur. Indeed, the case of an already diagonal H with equal eigenvalues fullfills this condition but possesses

two independent eigenvectors. We leave out this case since it leads to decoupled subsystems with trivial dynamics. Without loss of generality, we, thus, set $b \neq 0$. Introducing $\mu = c + \frac{\eta^2}{b}$, we obtain a convenient parametrization of nondiagonal complex 2×2 Hamiltonians,

$$H = \begin{pmatrix} \tau + \eta & b \\ \mu - \frac{\eta^2}{b} & \tau - \eta \end{pmatrix}, \tag{6}$$

whose eigenvalues collapse if and only if $\mu = 0$. We now enforce this restriction, making τ the only eigenvalue of H. Proceeding towards the Jordan normal form, we define

$$N := H - \tau \mathbb{I} = \begin{pmatrix} \eta & b \\ -\frac{\eta^2}{b} & -\eta \end{pmatrix}, \tag{7}$$

which is nilpotent as a direct computation shows. We can bring it to the canonical form using a similarity transform,

$$S^{-1}NS = \begin{pmatrix} \frac{1}{b} & 0 \\ \frac{\eta}{b} & 1 \end{pmatrix} N \begin{pmatrix} b & 0 \\ -\eta & 1 \end{pmatrix} = \begin{pmatrix} 0 & 1 \\ 0 & 0 \end{pmatrix}. \tag{8}$$

Applying the same transformation to the Hamiltonian yields its Jordan normal form

$$S^{-1}HS = \begin{pmatrix} \tau & 1 \\ 0 & \tau \end{pmatrix}, \tag{9}$$

where the single eigenvector associated with τ is given by

$$|\phi\rangle = \begin{pmatrix} b \\ -\eta \end{pmatrix}, \tag{10}$$

in the original basis. The time evolution of $|\phi\rangle$ then obeys Eq. (2); the eigenstate simply undergoes damped or amplified oscillations which leave the ratio of the two components unaffected, exactly as eigenstates in the diagonalizable case. The key difference with Hermitian time evolution is this: we can no longer express the time evolution of arbitrary states by projecting them on the eigenstates and evolve them separately since they do not span the full Hilbert space. The remainder of the Hilbert space did not disappear, we simply cannot compute the time evolution in this subsector the usual way.

B. Time evolution at the EP

To see what happens when the initial state is not fully aligned with the single eigenstate $|\phi\rangle$, we compute the evolution operator $U(t)$, a matrix exponential, by using the fact that the identity commutes with all other matrices. This allows us to use the Baker-Campbell-Hausdorff formula,

$$\begin{aligned} U(t) &= e^{-(it/\hbar)H} = e^{-(it/\hbar)(\tau\mathbb{I} + N)} = e^{-(it/\hbar)\tau\mathbb{I}} e^{-(it/\hbar)N} \\ &= e^{-(it/\hbar)\tau} \sum_{k=0}^{\infty} \frac{1}{k!} \left(-\frac{it}{\hbar}\right)^k N^k \\ &= e^{-(it/\hbar)\tau} \sum_{k=0}^{n} \frac{1}{k!} \left(-\frac{it}{\hbar}\right)^k N^k, \end{aligned} \tag{11}$$

where n is the order of the EP. An implicit version of this result was presented in Ref. [5]. For the Hamiltonian of Eq. (6), the

sum is cut off at $n = 1$ since $N^2 = 0$, but this formula is also valid for EPs of higher order. This yields the solution,

$$|\psi(t)\rangle = U(t)|\psi(0)\rangle = e^{(-i\tau/\hbar)t}\left(\mathbb{I} - \frac{it}{\hbar}N\right)|\psi(0)\rangle. \quad (12)$$

On one hand, we see that applying Eq. (12) to the coalesced eigenstate $|\phi\rangle$ yields the expected time evolution since $N|\phi\rangle = 0$. On the other hand, states that are not proportional to $|\phi\rangle$ generate components along $|\phi\rangle$ linearly in time as the image of N is spanned by $|\phi\rangle$. Arbitrary states, therefore, get closer and closer to the eigenstate as time passes. Time evolution at EPs, thus, differs from generic Hamiltonians in the sense that only one state evolves with the usual oscillations (possibly with overall damping or amplification), whereas other states remain inextricably coupled to this single eigenstate. In the case of a higher-order EP [Eq. (11)], this translates into a cascading temporal evolution where the generalized eigenvector of order k (a vector in the kernel of N^k but not of N^{k-1}) generates each generalized eigenvector of lower order according to a power law in time. Note that the highest power in time is associated with the generalized eigenvector of lowest order, namely, the EP eigenstate. This cascading evolution remains decoupled from generalized eigenstates of order higher than k; in particular, the coalesced eigenstate is the only one with fully decoupled dynamics. The only way to escape the EP eigenstate dominance as experimentally realized in Ref. [7] is to introduce a source, thus, rendering Eq. (1) inhomogeneous.

C. The four Möbius classes

How different can the situation be at a point close to the EP? Setting μ to be nonzero again, we find that the characteristic polynomial becomes

$$\chi(\lambda) = (\lambda - \tau)^2 - b\mu, \quad (13)$$

yielding the eigenvalues,

$$\lambda = \tau \pm \sqrt{b\mu}. \quad (14)$$

Interpreted as a function of μ, Eq. (14) defines the square-root Riemann surface that is often seen as the hallmark of EPs. Other parametrizations can lead to different eigenvalue surfaces [44]; selecting μ as a parameter has the added benefit of lifting the spectral degeneracy whereas keeping both the sum of the eigenvalues and the sum of the eigenvectors constant. Naturally, the splitting induced by μ also occurs at the eigenvector level with $|\phi\rangle$ turning into a pair of eigenvectors,

$$|\phi\rangle_\mu^\pm = |\phi\rangle \pm \begin{pmatrix} 0 \\ \sqrt{b\mu} \end{pmatrix}. \quad (15)$$

In principle, we now have a complete eigenbasis with simple time evolution on which we can project and evolve arbitrary states as in the Hermitian case. Nevertheless, the corresponding evolution operator relates continuously to the EP evolution operator. Indeed, an explicit computation yields

$$U_\mu(t) = e^{-(it/\hbar)H} = e^{(-i\tau/\hbar)t}\left[\cos\left(\frac{\sqrt{b\mu}}{\hbar}t\right)\mathbb{I} - \frac{it}{\hbar}\text{sinc}\left(\frac{\sqrt{b\mu}}{\hbar}t\right)N\right], \quad (16)$$

which reduces to the form given in Eq. (12) when $\mu \to 0$ with the leading term of the difference being linear in μ. To gain insight on the qualitative effect of this degeneracy lifting, we can start from the following observation: In general, nonzero values of $\sqrt{b\mu}$ will not only lead to a separation of eigenstates, but also dampen one of them and amplify the other due to the imaginary part of the eigenvalue. In this situation, any fluctuation away from the decaying eigenstate will, therefore, be amplified and tend to align more and more with the dominating eigenstate. We can make this statement quantitative by investigating the temporal evolution of the state's polarization. Defining the latter as $p(t) := \frac{\psi_2(t)}{\psi_1(t)}$, we get

$$p(t) = \frac{\psi_2(t)}{\psi_1(t)} = \frac{\left[\cos\left(\frac{\sqrt{b\mu}}{\hbar}t\right) + \frac{i\eta}{\sqrt{b\mu}}\sin\left(\frac{\sqrt{b\mu}}{\hbar}t\right)\right]p_0 + \left[\frac{i(\eta^2 - b\mu)}{b\sqrt{b\mu}}\sin\left(\frac{\sqrt{b\mu}}{\hbar}t\right)\right]}{\left[-\frac{ib}{\sqrt{b\mu}}\sin\left(\frac{\sqrt{b\mu}}{\hbar}t\right)\right]p_0 + \left[\cos\left(\frac{\sqrt{b\mu}}{\hbar}t\right) - \frac{i\eta}{\sqrt{b\mu}}\sin\left(\frac{\sqrt{b\mu}}{\hbar}t\right)\right]}, \quad (17)$$

which constitutes a time-dependent Möbius transformation of the initial polarization p_0 as previously shown in Ref. [42] for $\eta = 0$ Hamiltonians. Such transformations are elements of the Möbius group. After properly normalizing the factors appearing in Eq. (17), we can use the square of the trace of the associated matrix [22] to classify the transformation: $\sigma := \text{Tr}^2(U/e^{(-i\tau/\hbar)t}) = 4\cos^2(\frac{\sqrt{b\mu}}{\hbar}t)$. The Möbius group then splits into four classes:

(1) The *hyperbolic* class [Fig. 1(a)] corresponds to σ real with $\sigma > 4$. For $b\mu$ real and negative, the transformation is hyperbolic at all times. In this case, all initial polarizations converge towards the attractive eigenstate along direct arcs with the exception of an unstable initial condition corresponding to the repulsive eigenstate.

(2) The *elliptic* class [Fig. 1(b)] corresponds to σ real with $\sigma < 4$. For $b\mu$ real and positive, the transformation

stays elliptic at all times except for the periodic return to the initial polarization. This case is the most Hermitian-like: All polarizations oscillate in time and no eigenvector dominates.

(3) The *loxodromic* class [Fig. 1(c)] is the most generic one; it occurs for $\text{Im}(\sigma) \neq 0$. For complex $b\mu$, the transformation stays loxodromic almost all the time except for isolated hyperbolic points that occur for $\text{Re}(\frac{\sqrt{b\mu}}{\hbar}t) = n\frac{\pi}{2}$, $n \in \mathbb{N}$. This class can be considered as an intermediary between elliptic and hyperbolic classes. As in the latter case, one eigenstate dominates, but the trajectories are now spiraling to some degree.

(4) The *parabolic* class [Fig. 1(d)] arises for nonidentity transformations with $\sigma = 4$. This occurs when the two fixed points of the other classes merge, which happens for $b\mu = 0$; we then have an EP and the system stays parabolic at all times.
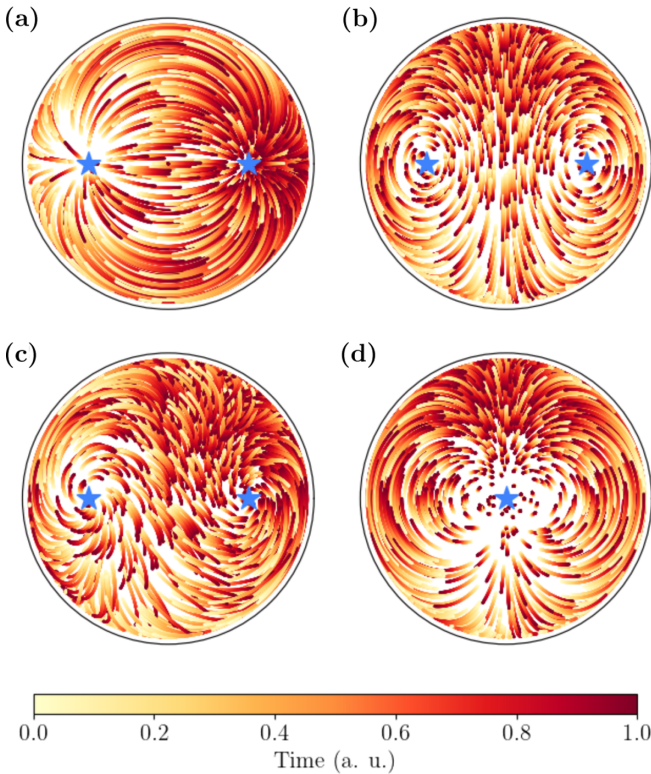
FIG. 1. The coalescence of polarization. Stereographic projection on the top hemisphere of the Poincaré sphere with 1000 random initial polarizations evolving under a Hamiltonian that corresponds to (a) hyperbolic, (b) elliptic, (c) loxodromic, (d) parabolic Möbius transformations, respectively. The polarizations of the eigenvectors are marked with blue stars.

All polarizations eventually converge to the unique fixed point corresponding to the coalesced eigenstate.

The value of $b\mu$, therefore, largely determines the nature of the Möbius transformation that acts on the polarization. Hence, we will term the Hamiltonians themselves hyperbolic, elliptic, parabolic, and loxodromic depending on the value of $b\mu$. In terms of the original Hamiltonian of Eq. (3), the EP occurs when the product of the coupling terms bc matches the square of the detuning $(\frac{a-d}{2})^2$ with the correct phase and amplitude. If this condition is not met, the coalesced eigenstate can split in three different ways: elliptic, hyperbolic, and loxodromic. Let us focus on the latter two, which correspond to the generic case of $\text{Im}(\sqrt{b\mu}) \neq 0$. Using $\lim_{t\to\infty} \tan(\frac{\sqrt{b\mu}}{\hbar}t) = \pm i$, we get

$$\lim_{t\to\infty} p(t) = \lim_{t\to\infty} \frac{b\sqrt{b\mu}\,p_0 + i(bp_0\eta + \eta^2 - b\mu)\tan\left(\frac{\sqrt{b\mu}}{\hbar}t\right)}{b\sqrt{b\mu} - ib(bp_0 + \eta)\tan\left(\frac{\sqrt{b\mu}}{\hbar}t\right)}$$
$$= \frac{-\eta \pm \sqrt{b\mu}}{b}, \tag{18}$$

which corresponds to the polarization of the dominating eigenstate, namely, the one with the eigenvalue of largest positive imaginary part. As in the parabolic (EP) case, the long-term fate of the polarization does not depend on the initial condition for these generic non-Hermitian

Hamiltonians, unless the system is initialized exactly in the repulsive eigenstate of the system.

What about the nongeneric cases we set aside? They correspond to $\mu = sb^*$ with s real. Recalling Eq. (14), we see that the spectrum is either purely real in the elliptic case or consists of a complex-conjugate pair in the hyperbolic case. It was shown in Ref. [9] that Hamiltonians have such spectra if and only if they commute with an invertible antilinear operator A,

$$[H, A] = 0, \tag{19}$$

which is also equivalent to the property of *pseudo-Hermiticity*, introduced in Ref. [10]. In the particular case of parity-time ($\mathcal{PT}$) symmetry [8], the hyperbolic and elliptic classes, respectively, are known as "$\mathcal{PT}$-broken" and "$\mathcal{PT}$-unbroken" phases. Other antilinear symmetries, such as anti-$\mathcal{PT}$ symmetry [45], can play the same role.

In addition to the polarization effects we discussed at length, we must also mention that for $\tau = 0$, the imaginary parts of the eigenvalues lead to an exponential growth in the loxodromic and hyperbolic classes. The parabolic class presents a different instability due to the linearly growing term in Eq. (12). Introducing an imaginary part in τ can stabilize all of these cases.

D. The higher-dimensional case

How does this Möbius transformation approach generalize to larger Hamiltonians? Consider the neighborhood of an EP of arbitrary order n. In the case of nth root splitting of the eigenvalue τ—the case typically considered in sensing applications—the characteristic polynomial can be written as

$$\chi(\lambda) = (\tau - \lambda)^n - \gamma^n = 0, \tag{20}$$

leading to the n eigenvalues $\lambda = \tau + \gamma e^{im2\pi/n}$, where $m \in [0, n-1]$. Since all eigenvalues are different, the corresponding Hamiltonian is diagonalizable and can be brought into the form

$$H = \begin{pmatrix} \tau & 1 & & & & \\ & \tau & 1 & & & \\ & & \tau & \ddots & & \\ & & & \ddots & 1 & \\ & & & & \tau & 1 \\ \gamma^n & & & & & \tau \end{pmatrix}, \tag{21}$$

through a similarity transform. Equation (16) then readily generalizes through the introduction of the following functions:

$$K(n, m, z) = \frac{1}{n}\sum_{k=0}^{n-1} e^{imk(2\pi/n)} e^{ik(2\pi/n)z}, \tag{22}$$

which are generalizations of the hyperbolic sine and cosine that are symmetric under the action of the cyclic group of order n. The idea that underlies our definition is analogous to the standard process of symmetrizing multivariate functions under permutation of their arguments, by averaging the function over the symmetric group [46]. Our K functions can also

be seen as the discrete Fourier transform [47] of the image of the n roots of unity under an exponential map. In Appendix A, we discuss this in more detail, along with other properties of K functions. Most importantly, these functions allow us to compute the evolution operator for the Hamiltonian of Eq. (21)

$$U(t) = e^{-(it/\hbar)H} = e^{-(it/\hbar)[\tau+(H-\tau)]} = e^{-(it/\hbar)\tau}e^{-(it/\hbar)(H-\tau)}$$

$$= e^{-(it/\hbar)\tau}\sum_{m=0}^{n-1} K(n,-m,-i\gamma t)\left(\frac{H-\tau}{\gamma}\right)^m, \qquad (23)$$

where we used $(H-\tau)^{n+1} = \gamma^n$. As for Eq. (16), the EP case of Eq. (11) arises when taking the limit $\gamma \to 0$. Component-wise, Eq. (23) reduces to the simple form

$$U_{pq}(t) = \gamma^{p-q}K(n, p-q, -i\gamma t)e^{-(it/\hbar)\tau}, \qquad (24)$$

which is useful to investigate polarization properties. We now define $n-1$ such polarizations with respect to the first component of our state vector as $p_k(t) := \frac{\psi_k(t)}{\psi_1(t)}$. The temporal evolution of these polarizations is then given by

$$p_k(t) = \frac{\sum_{q=1}^{n} U_{kq}(t)p_q(0)}{\sum_{j=1}^{n} U_{1j}(t)p_j(0)}, \qquad (25)$$

which still constitutes a Möbius transformation of $p_k(0)$ but now also depends on the other polarizations, preventing a direct classification as in the two-level case. Nevertheless, we can investigate the long-term behavior by adapting the strategy of Eq. (18). We start by introducing higher-order equivalents of the tangent function,

$$T(n,m,z) = K(n,m,z)/K(n,0,z). \qquad (26)$$

The graph of a T function is depicted in Fig. 2. It highlights a useful property: for θ in the jth sector, which we define as $\frac{j2\pi}{n} - \frac{\pi}{n} < \theta < \frac{j2\pi}{n} + \frac{\pi}{n}$, we have the limit,

$$\lim_{t\to\infty} T(n,m,e^{i\theta}t) = e^{-imj(2\pi/n)}, \qquad (27)$$

which makes Eq. (25) time independent; indeed, we can write

$$p_k(t) = \frac{\sum_{q=1}^{n} \gamma^{k-q}T(n,k-q,-i\gamma t)p_q(0)}{\sum_{l=1}^{n} \gamma^{1-l}T(n,1-l,-i\gamma t)p_l(0)}. \qquad (28)$$

For $\arg(-i\gamma)$ in the jth sector, this yields

$$\lim_{t\to\infty} p_k(t) = \frac{\sum_{q=1}^{n}(\gamma e^{-i(j2\pi/n)})^{k-q}p_q(0)}{\sum_{l=1}^{n}(\gamma e^{-i(j2\pi/n)})^{1-l}p_l(0)}$$

$$= (\gamma e^{-i(j2\pi/n)})^{k-1}. \qquad (29)$$

which shows that time evolution is dominated by a single fixed point in the generic (loxodromic) case $\arg(-i\gamma) \neq \frac{j2\pi}{n} + \frac{\pi}{n}$ for some integer j. As in the second-order case, an exception occurs when $\arg(-i\gamma)$ is at the interface between two sectors; we then recover elliptic behavior in the long term. To prove this, we select $-i\gamma = e^{-i(\pi/n)}g$ with g real and leverage another property of T functions, namely,

$$T(n,m,e^{-i(\pi/n)}gt)$$

$$\approx e^{im(\pi/n)}\left\{\cos\left(\frac{\pi}{n}\right) - \tan\left[\sin\left(\frac{\pi}{n}\right)gt\right]\sin\left(m\frac{\pi}{n}\right)\right\}$$
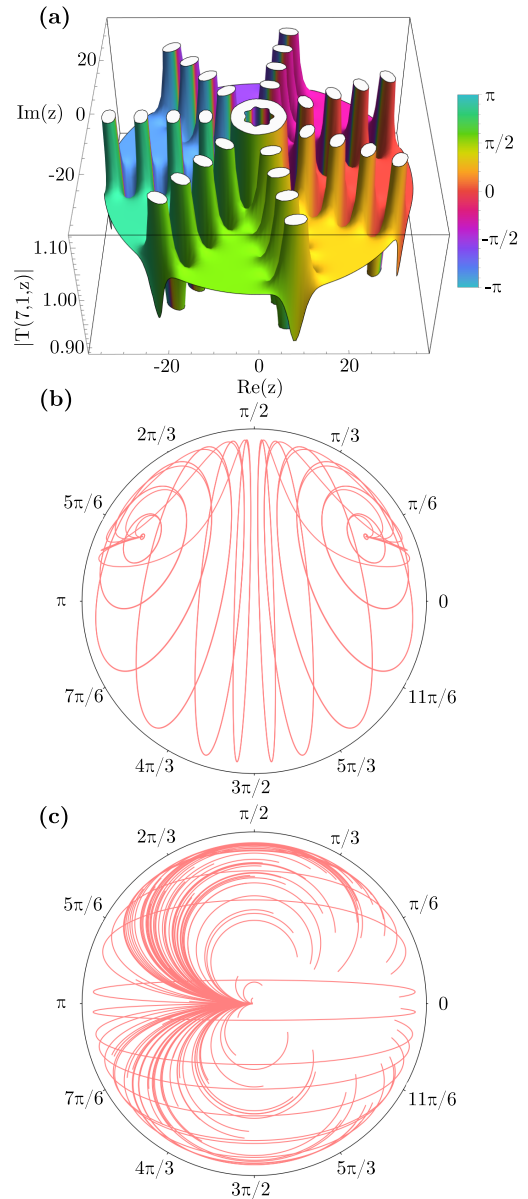
$$\qquad (30)$$

(a)

(b)

(c)

FIG. 2. Möbius transform in higher dimensions. (a) Plot of the $T(7, 1, z)$ function with colors encoding the phase of the function. (b) Projection of the $p_2(t)$ polarization on the Poincaré sphere for a third-order elliptic Hamiltonian with $p_2(0)$ lying on the fixed points and $p_3(0)$ deviating from the fixed point condition. (c) Projection of the $p_3(t)$ polarization on the Poincaré sphere for a third-order EP with $p_3(0)$ randomly distributed in a square domain with corners $\pm(1 + i)$ and $p_2(0) = 0$.

for $gt \gg 1$. Insertion in Eq. (28) then reveals that at times sufficiently larger than $\frac{1}{g}$, the polarizations become periodic with angular frequency $\sin(\frac{\pi}{n})g$. Furthermore, the initial conditions $p_k(0) = \gamma^{k-1}$ and $p_k(0) = (\gamma e^{i(2\pi/n)})^{k-1}$ cancel out the time dependency altogether and correspond to the two fixed points of the system. An example of such higher-order elliptic evolution is provided in Fig. 2(b), which depicts the evolution of $p_2(t)$ in a third-order system with $\mu = \frac{1}{2}e^{i\pi/n/2(n-2)}$ and $p_2(0) = \frac{1}{2}e^{i\pi/n/2(n\pm2)}$, which corresponds to the fixed points of the system. The variations in the trajectories come from

$p_3(0) = (\frac{1}{2}e^{i\pi/n/2(n\pm 2)})^2 + s$ deviating from the fixed point condition by some amount s. The value of s determines the final circle on which the trajectory stabilizes. In Fig. 2(b), the trajectories associated with 14 different values of s are depicted.

Finally, we turn to the parabolic case. At the EP, time evolution follows Eq. (11). If the state vector deviates from the single eigenstate only in the kth component, we have $p_j(0) = 0 \; \forall \; j \neq k$ and

$$p_k(t) = \frac{p_k(0)}{\frac{1}{k!}\left(\frac{-it}{\hbar}\right)^k p_k(0) + 1}, \qquad (31)$$

which is a parabolic transformation of the initial deviation $p_k(0)$. The evolution speed and preferred direction towards the fixed point change depending on k. When more than one initial polarization is nonzero, these convergence patterns enter in competition, adding a transient response that deforms the curves, but the attractive parabolic fixed point remains unique. Hence, Möbius classes are relevant at higher order; the loxodromic class occurs generically when μ lies within a sector. When μ falls precisely at the interface between two sectors, we have the elliptic case. Finally, the parabolic case occurs for $\mu = 0$. The additional degrees of freedom due to the higher order add a layer of complexity to these polarization transformations.

III. FLOQUET NON-HERMITIAN HAMILTONIANS

So far, we have studied non-Hermitian time evolution both at EPs and under nth root splitting of the eigenvalues. However, some of the most interesting properties of EPs only arise when the parameters of the Hamiltonian are modulated in order to move around the Riemann surfaces associated with such splittings. In particular, EP encircling has been shown to result in asymmetric mode switching [17]. On the other hand, Eqs. (18) and (29) show that the closely related property of polarization convergence is a rather general feature of non-Hermitian Hamiltonians; It is, therefore, natural to explore the repartition of Möbius classes under such temporal modulations to see whether EP encircling impacts the Möbius class in some way. To do so, we derive exact solutions for time evolution under periodically modulated Hamiltonians and interpret them in terms of the Möbius group. The modulations we will study keep the EP Riemann surface fixed with $\mu(t)$ and $\eta(t)$ describing some trajectories on the complex plane. Without loss of generality, we can set $\tau = 0$ since it only gives rise to an exponential prefactor. We then rewrite Eqs. (1) and (6) as

$$i\hbar \, \partial_t \eta \, \psi_1 = i\hbar(\partial_t \eta)\psi_1 + \eta^2 \psi_1 + b\eta\psi_2, \qquad (32)$$

$$i\hbar \, \partial_t b \, \psi_2 = b\mu\psi_1 - \eta^2 \psi_1 - b\eta\psi_2, \qquad (33)$$

which we sum to obtain

$$p(t)\psi_1 = -\hbar^2 \partial_t^2 \psi_1, \qquad (34)$$

where $p(t) := b\mu + i\hbar \, \partial_t \eta$. One can treat cases where τ and b are also time modulated in an analogous manner, but this will, in general, give rise to an additional damping term. For periodic modulations, Eq. (34) is the Hill equation [48], which
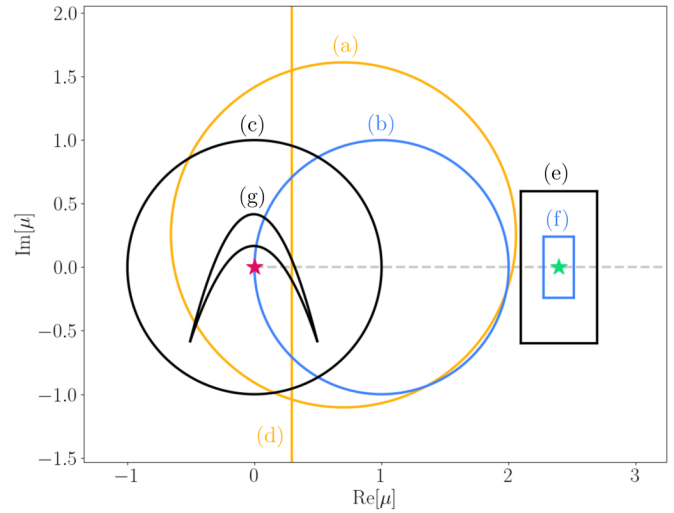

FIG. 3. Time modulation curves. Circular (a)–(c), rectangular (d)–(f), and quadratic (g) modulation curves. The yellow curves lead to loxodromic evolution, the black curves lead to parabolic evolution, and the blue curves lead to elliptic evolution. The time-independent EP is denoted by a red star. The rectangular curves have the same aspect ratio and center, the latter being marked with a green star. The gray dashed line corresponds to $\text{Im}(\sqrt{\mu}) = 0$.

has no general closed-form solutions. A particularly important subcase is Mathieu's equation [49], which corresponds to a purely real cosine modulation, giving rise to the phenomenon of parametric resonance [50]. Since our motivation lies in EP encircling, we consider modulations that describe loops on the complex plane, instead, with segments for which Eq. (34) has analytical solutions. For any such segment, we obtain two solutions ψ_1 and ψ_1'. As for ψ_2 and ψ_2', they can be evaluated from ψ_1 through Eq. (32). From these solutions, we then build a fundamental matrix,

$$\Psi(t) := \begin{pmatrix} \psi_1(t) & \psi_1'(t) \\ \frac{i\hbar}{b}\partial_t \psi_1(t) - \frac{\eta}{b}\psi_1(t) & \frac{i\hbar}{b}\partial_t \psi_1'(t) - \frac{\eta}{b}\psi_1'(t) \end{pmatrix}, \qquad (35)$$

from which the evolution operator follows:

$$U(t) = \Psi(t)\Psi^{-1}(0). \qquad (36)$$

If the modulation changes after a time t_c elapsed, the overall evolution operator becomes

$$U(t) = [1 - \Theta(t - t_c)]U_a(t) + \Theta(t - t_c)U_b(t)U_a(t_c), \qquad (37)$$

where U_a and U_b, respectively, are the evolution operators associated with the first and second phases of the modulation. We can, therefore, form solutions for a large variety of piecewise defined modulation curves on the complex plane. In general, a given second-order differential equation can be realized by infinitely many different Hamiltonians, corresponding to different choices of μ and η. For the sake of simplicity, we will, therefore, set $\eta = 0$ from now on, keeping in mind that U can be deformed using Eqs. (34) and (35) to accommodate for a time-dependent detuning η.

We apply this method to three different families of periodically time-modulated Hamiltonians with modulation curves that are constituted of circular [Figs. 3(a)–3(c)], linear

[Figs. 3(d)–3(f)] and quadratic [Fig. 3(g)] segments. The corresponding solutions to Eq. (34) are Bessel, Airy, and parabolic cylinder functions, respectively [51].

Möbius classes in the Floquet setting

Floquet's theorem [52] tells us that for such periodically modulated Hamiltonians, the evolution operator decomposes as $U(t) = Q(t)e^{Bt}$, where $Q(t)$ has the same periodicity as the modulation and B is a constant matrix. The long-term behavior of the system is, therefore, determined by the nonperiodic envelope e^{Bt}, which has the same form as the evolution operator for time-independent Hamiltonians. Hence, we can also classify Floquet non-Hermitian systems in terms of the Möbius group by diagonalizing the exact expression from Eq. (36) (a representative example is given in Appendix B). In the following, λ_F will denote the logarithm of the eigenvalues of $U(t)$ after one period; we will refer to this quantity as a *Floquet exponent* of the system. Since this quantity is only defined up to a multiple of $2\pi i$, we need to exercise special care when the Floquet exponents coincide; in this situation, the eigenvectors determine whether the parabolic class occurs or not. We start with a modulation curve commonly considered in theoretical studies, namely, a circular modulation [Figs. 3(a)–3(c)], which has the form

$$\mu(t) = \Delta + \rho e^{i\omega t}. \qquad (38)$$

It can be solved in terms of Bessel functions as performed in Ref. [39]. Diagonalizing U in Eq. (36) yields a particularly simple result in the circular case; the Floquet exponents evaluate to $\lambda_F = \sqrt{b\Delta}$. This reveals that the time-dependent case is in close correspondence to the static one, in the sense that the Möbius class solely depends on the modulation center for circular curves and that this dependency has the same form as in the static case. As we will later see, this correspondence completely breaks down for noncircular modulation curves. This dependency on Δ reveals that generic parameters [Fig. 3(a)] lead to loxodromic evolution. In this case, the dominant eigenstate expands following a logarithmic spiral [Fig. 4(a)], whereas the other eigenstate spirals towards the origin [Fig. 4(b)].

Most modulation curves that are centered on the positive real axis lead to stable trajectories, which can be periodic [Figs. 3(b), 4(c), and 4(d)] or form rosettes for irrational Floquet exponents. In particular, periodic trajectories can have periods much larger than the modulation. As shown by Berry and Uzdin in [39], additional Floquet EPs occur when the Floquet exponents become multiples of π. When the modulation circle is centered on the static EP, we get a Floquet EP [Figs. 3(c), 4(e), and 4(f)], regardless of the radius and modulation frequency. In Fig. 4(e), we see that the eigenstate describes a cycle on the complex plane with every modulation period. In line with our earlier description of the time-independent case, Fig. 4(f) shows that other states tend to acquire the polarization of the eigenstate, leading to a characteristic Archimedean spiral pattern.

Crucially, the modulation depth ρ does not affect the Floquet exponents. However, it does impact the periodic component of the time-evolution $Q(t)$. For instance, if the modulation curve is a decentered loop that dynamically
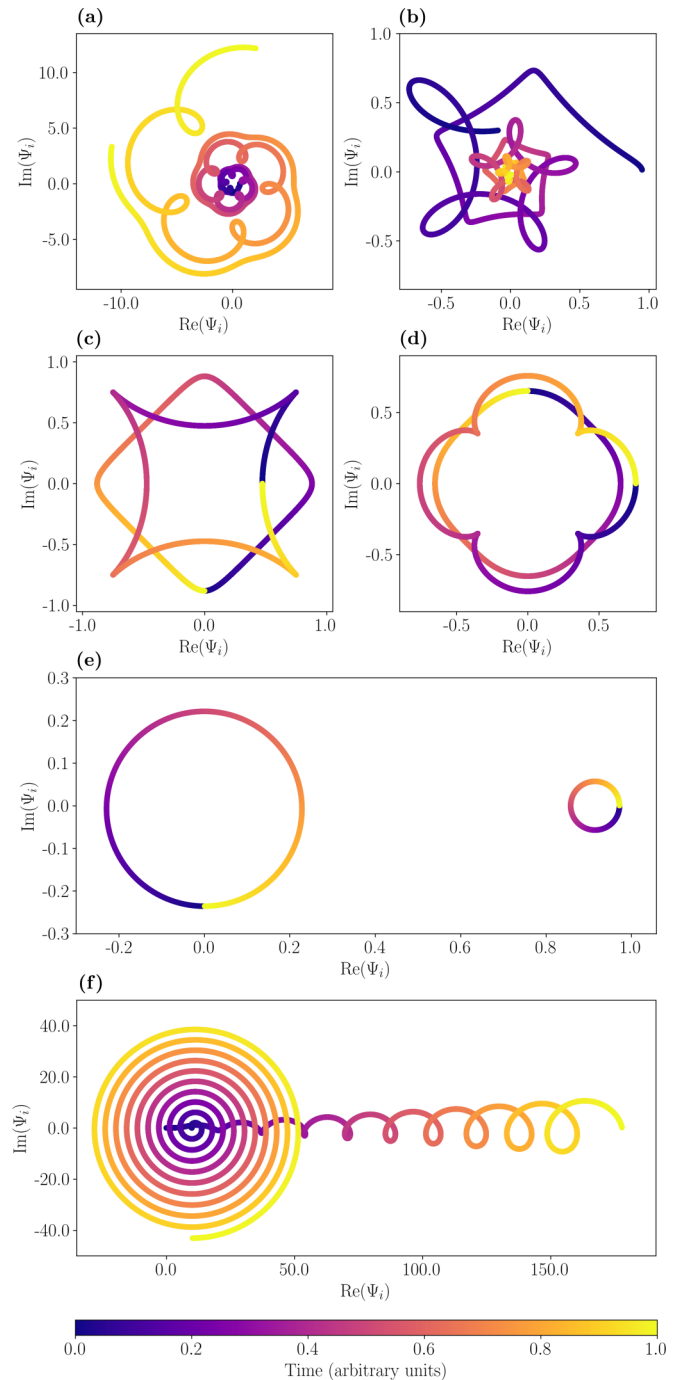

FIG. 4. Circular modulations. (a)–(e) Time evolution of stroboscopic eigenstates for various parameters. (a) and (b) Noncentered EP encircling with $\Delta = 0.700\,145 + 0.254\,176i$ and $\rho = 1.357\,497$. (c) and (d) Loop crossing the static EP $\Delta = \rho = 1$. (e) Centered EP encircling, with $\Delta = 0$ and $\rho = 1$. (f) Evolution of a noneigenstate under the same parameters. The state's two components are represented in each plot with time encoded as color.

crosses the static EP [Fig. 3(b)], the evolution presents a cusp point at the time for which the EP condition is met [Figs. 4(c) and 4(d)]. For larger radii, the cusps turn into self-intersections [Figs. 4(a) and 4(b)]. This is not a topological property since self-intersections can be created in other ways.

Is the Möbius class always neatly determined by the modulation center Δ as in the circular case? To answer this question, we consider a time modulation with linear segments, which can be solved in terms of Airy functions. Our example comprises four such segments, defined by

$$\mu_a(t) = \Delta - \frac{\rho}{2} + i\alpha\frac{\rho}{2} + \rho t, \tag{39}$$

$$\mu_b(t) = \Delta + \frac{\rho}{2} + i\alpha\frac{\rho}{2} - i\alpha\rho t, \tag{40}$$

$$\mu_c(t) = \Delta + \frac{\rho}{2} - i\alpha\frac{\rho}{2} - \rho t, \tag{41}$$

$$\mu_d(t) = \Delta - \frac{\rho}{2} - i\alpha\frac{\rho}{2} + i\alpha\rho t, \tag{42}$$

which build a rectangle; Figs. 3(d)–3(f)] of aspect ratio α and width ρ. Fixing the modulation depth at $\Delta = 2.394\,756\,696$, we vary ρ. For $\rho = 4.2$ [Figs. 3(d), 5(a), and 5(b)], the evolution is of the hyperbolic type. For $\rho = 0.6$ [Figs. 3(e), 5(c), and 5(d)], we get the parabolic type, and finally for $\rho = 0.24$ [Figs. 3(f), 5(e), and 5(f)], we get elliptic evolution. The modulation depth clearly impacts the Möbius class of rectangular modulations, and the Floquet exponents do not assume a practical closed form.

We have seen that under both circular and rectangular modulations, Floquet EPs can occur far away from the static EP without encircling it. We can complete the picture by showing that Floquet EPs can also arise for nonencircling trajectories in the direct vicinity of the static EP. To that end, and in order to demonstrate a third family of exact solutions, we consider a concave modulation curve made of two quadratic segments,

$$\mu_a(t) = \Delta - (1+i)/2 + (1+4i)t - 4it^2, \tag{43}$$

$$\mu_b(t) = \Delta - (1+i)/2 + (1+3i)(2-t) - 3i(2-t)^2. \tag{44}$$

This case is solved in terms of parabolic cylinder functions. For $\Delta = -0.005\,861\,59 - 0.083\,075\,2i$ [Fig. 3(g)], we obtain a Floquet EP without encircling the static EP. Indeed, the system possesses a single eigenstate [Fig. 5(g)], whereas noneigenstate initial conditions lead to an Archimedean-spiral-like behavior [Fig. 5(h)] that stroboscopically tends towards a unique fixed point in polarization.

With these various examples, we have shown that the Möbius class, which captures the nature of the time evolution, is logically decoupled from EP encircling. The latter does not seem to be a particularly relevant parameter in understanding time evolution under modulated non-Hermitian Hamiltonians, apart from creating cusps in the resulting trajectories. In the next section, we show that such phenomena are better understood in terms of parametric resonance.

IV. COMPLEX PARAMETRIC RESONANCE

The close correspondence between the static and the circular Floquet case is atypical; the other cases we studied hint at a much more intricate distribution of Möbius classes with the latter depending on the modulation depth [Figs. 5(a)–5(f)] and hyperbolic Floquet systems sometimes occurring for Δ real and positive [Figs. 5(a) and 5(b)]. We now study these distributions in more detail by comparing stability diagrams
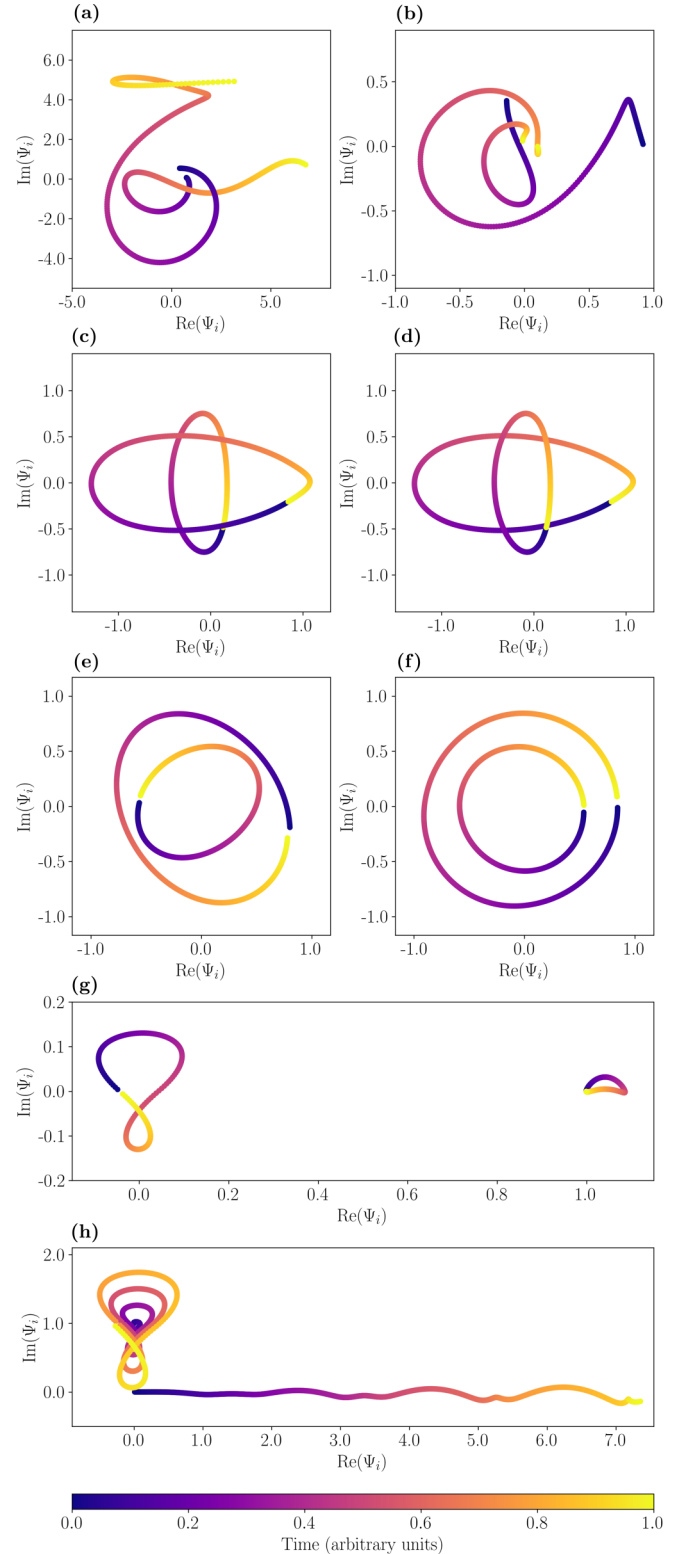

FIG. 5. Noncircular modulations. (a)–(f) Time evolution under rectangular modulations with $\Delta = 2.394\,756\,696$, $\alpha = 2$ and varying modulation depth: (a) and (b) stroboscopic eigenstates with $\rho = 4.2$ [Fig. 3(d)]. (c) and (d) Two degenerate eigenstates for $\rho = 0.6$ [Fig. 3(e)]. (e) and (f) stroboscopic eigenstates with $\rho = 0.24$ [Fig. 3(f)]. (g) Single eigenstate for the quadratic curve of Fig. 3(g). (h) Evolution of a noneigenstate under the same modulation. The state's two components are represented in each plot with time encoded as color.
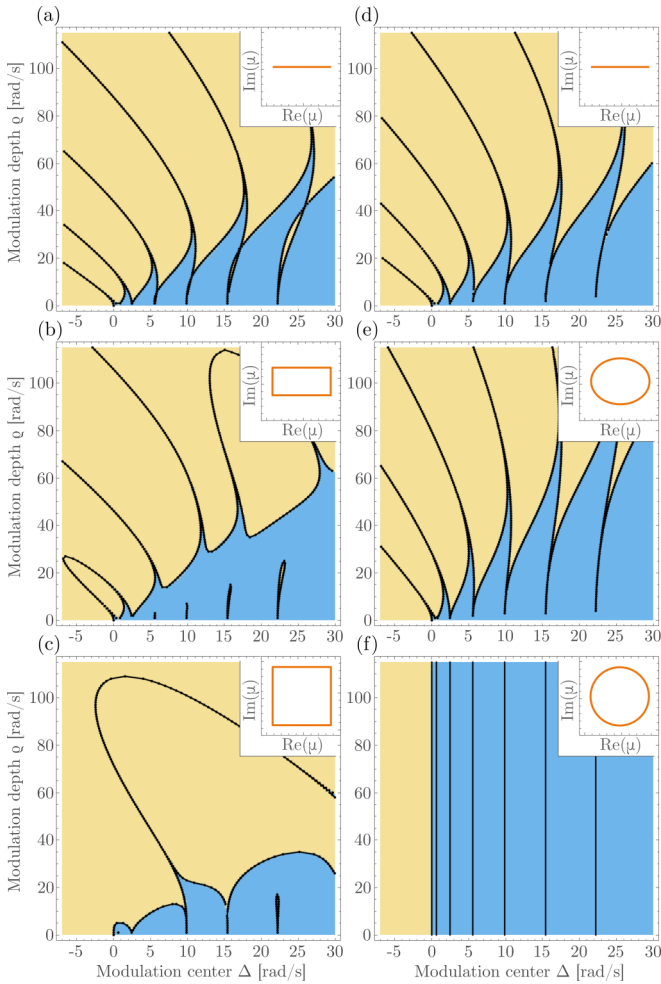
FIG. 6. Complex parametric resonance. Stability diagrams for rectangular (a)–(c) and elliptic (d)–(f) modulations of varying aspect ratios. Black points denote EPs. The blue regions are in the stable (elliptic) phase, whereas the yellow regions are in the unstable (hyperbolic) phase. The aspect ratios are $\alpha = 0$ (a), $\alpha = 0.475$ (b), $\alpha = 1.0$ (c), $\alpha = 0.0$ (d), $\alpha = 0.8$ (e), and $\alpha = 1.0$ (f). The corresponding modulation curves are represented in the insets.

for modulation curves describing rectangles [Figs. 6(a)–6(c)] and ellipses [Figs. 6(d)–6(f)] on the complex plane. Since we mapped the problem to Hill's equation, we can leverage the associated literature [43,50,53,54] to identify features that are exclusive to complex modulation curves.

We start with a rectangular trajectory chosen to mimic Mathieu's equation by setting the aspect ratio to $\alpha = 0$. The modulation is then purely real and approximates a cosine. The corresponding stability diagram [Fig. 6(a)] is qualitatively similar to the one obtained for a purely real cosine modulation [Fig. 6(d)], which is known as a Strutt diagram [50]. Both exhibit the essential features of parametric resonance, namely, domains of stability (blue, elliptic) and instability (yellow, hyperbolic) that interpenetrate through several very thin "*tongues*" of instability (respectively, stability.), whose boundaries (black lines) correspond to Floquet EPs. Only one essential difference appears: In the rectangular case, the instability tongues all present a self-crossing (a *coexistence* [43]) of their two EP boundaries.

We then introduce an imaginary part in the modulation curves [Figs. 6(b) and 6(e)]. In Fig. 6(b), we show the case of a rectangular modulation with an aspect ratio of $\alpha = 0.475$. The stability diagram shows many nontrivial features, which now differ substantially from the ones observed in standard parametric resonance; for instance, some of the stability tongues are no longer shooting off to infinity but instead form an arch merging at some finite modulation depth. Similar structures have been reported in Ref. [55] for $\mathcal{PT}$-symmetric scattering systems. Interestingly, the presence of, at least, the first of these arches is demonstrably forbidden for real modulations and, therefore, constitutes a signature of complex parametric modulation. Indeed, Theorem 4.4 in Ref. [43] (due to Borg [54]) guarantees the existence of a strictly negative first interval of instability for all nonzero modulation depths (the "inverted pendulum" interval). Furthermore, the oscillation theorem (Theorem 2.1 in Ref. [43], originally due to Lyapunov [53]) tells us that no interval of stability exists for negative modulation centers exceeding the modulation depth. The instability region directly above the first arch is incompatible with these requirements, and such an arch could, therefore, not occur for purely real time modulations.

Another remarkable change consists in the disappearance of the coexistence points that were present in the instability tongues of Fig. 6(a), splitting each instability tongue in an isolated domain within the now fully connected stable region and a part connecting to the larger instability domain. We conjecture that this also constitutes a signature specific to complex modulations.

In contrast, the effect of a nonzero aspect ratio is much simpler when the modulation follows an ellipse on the complex plane: Fig. 6(e) shows the stability diagram for an aspect ratio of 0.8. The only effect is a vertical stretching of the diagram that extends the reach of stability, ultimately culminating in the ρ-independent stability diagram observed in Fig. 6(f), which corresponds to the $\sqrt{b\Delta}$ Floquet exponents of the last section. This explains how parametric resonance is hidden in the specific case of circular modulation curves. It also implies even a slight flattening of the circular trajectory introduces parametric instability in the system with finite hyperbolic intervals appearing. This behavior is unusual; for real modulations, stability diagrams of the type depicted in Fig. 6(f) are forbidden. Indeed, the oscillation theorem implies that *"neither an interval of stability nor an interval of instability can ever shrink to a point"* (p. 14 in Ref. [43]). In addition, the only real periodic function for which all intervals of instability vanish is the constant function (Theorem 7.12 in Ref. [43], first in Ref. [54]), which adds to the peculiarity of the complex circular modulation.

If we try to imitate the circular case by selecting a square time modulation ($\alpha = 1$), something entirely different happens. The non-Hermitian stability features already observed in Fig. 6(b) are only reinforced in Fig. 6(c). The number of stability tongues is reduced, giving way to a larger instability domain. An accompanying movie [56] shows the continuous transition from Figs. 2(a) to 2(c); it exhibits intricate interactions between the stability tongues as the height of the rectangular loop increases.

Given their atypicality, the use of circular trajectories in theoretical studies is rather unfortunate: for instance, one

cannot hope to emulate a theoretical result based on circular modulation through an experiment employing a rectangular modulation as the two differ greatly in their qualitative behavior. Furthermore, even if circular loops were experimentally accessible, parametric resonance would creep back in at the slightest departure from circularity. Parametric resonance clearly needs to be accounted for in theoretical treatments of EP encircling.

V. CONCLUDING REMARKS

First, we have shown how the peculiar cascading temporal dynamics of EPs relate continuously to that of neighboring nonexceptional points. Classifying the possible temporal behaviors with the Möbius group illuminates the position of EPs within the larger landscape of non-Hermitian Hamiltonians and complements the usual approach based on restricting the parameter space through an antilinear symmetry.

This led to our main result: Together with an analytical approach that highlights the connection to parametric resonance, these classes allowed us to make sense of non-Hermitian time-modulated systems. First, we have shown that encircling is not related to the long-term behavior of the system; it is relevant to the periodic part of the dynamics where it induces the formation of self-intersections. Instead, we found that the repartition of temporal Möbius classes constitutes a complex parametric resonance phenomenon whose qualitative features greatly depend on the shape of the modulation curve. Our explicit link to Hill's equation allowed us to delineate specific signatures of complex parametric resonance: stability arches and splitting coexistence points. Furthermore, we could show that the choice of a single-frequency circular modulation artificially conceals parametric resonance features; this phenomenon is also unique to complex modulations. Further research on that front could identify other restrictions of real parametric resonance that are lifted in the complex realm; this is especially interesting, given the numerous applications of parametric oscillators. On another front, applying our theory in a fully quantum setting calls for a Lindblad formulation in order to account for quantum fluctuations [57]. Yet another potential direction for future research lies in further exploration of higher-order Hamiltonians. In the unmodulated case, this would mean considering different eigenvalue splittings. In the modulated case, one could consider equations with higher-order derivatives. There are many exciting prospects both in further exploration of the puzzling features of complex parametric resonance and on the possibility of synthesizing Floquet EPs through designed modulation schemes.

ACKNOWLEDGMENTS

APPENDIX A: PROPERTIES OF K FUNCTIONS

In this Appendix, we discuss some of the properties of the K functions introduced in Eq. (22). As a starting point, note

that the hyperbolic cosine and sine are the even and odd part of the exponential function, respectively. A fruitful alternative is to think of cosh as being invariant under a rotation of its argument by π, whereas sinh picks up a $e^{i\pi}$ phase under the same rotation. The K functions introduced in Eq. (22) can then be interpreted as C_n-symmetric generalizations of trigonometric functions. Indeed, they satisfy the following symmetry property:

$$K(n, m, e^{i(2\pi/n)}z) = e^{-im(2\pi/n)}K(n, m, z). \qquad (A1)$$

In particular, $K(n, 0, z)$ is invariant under rotations by $\frac{2\pi}{n}$ and generalizes the hyperbolic cosine function. Other properties of hyperbolic functions admit a generalization. For instance, we have

$$\sum_{m=0}^{n-1} K(n, m, z) = e^z. \qquad (A2)$$

As a consequence, the equivalent of $\cosh^2 - \sinh^2 = 1$ becomes

$$\left[\sum_{m=0}^{n-1} K(n, m, z)\right]\left[\sum_{m=0}^{n-1} K(n, m, -z)\right] = 1. \qquad (A3)$$

As for derivation rules for sinh and cosh, they generalize as

$$\partial_z K(n, m, z) = K(n, m+1, z), \qquad (A4)$$

which also constitutes a closed chain of derivatives, keeping in mind that

$$K(n, m+n, z) = K(n, m, z). \qquad (A5)$$

Finally, we mention an interesting connection to the discrete Fourier transform: indeed, if we write $\alpha := e^{i(2\pi/n)}$ and collect the definitions of the K functions of order n in a single matrix equation, we obtain

$$n\begin{pmatrix} K(n, 0, z) \\ K(n, 1, z) \\ K(n, 2, z) \\ \vdots \\ K(n, n-1, z) \end{pmatrix}$$

$$= \begin{pmatrix} 1 & 1 & 1 & \dots & 1 \\ 1 & \alpha & \alpha^2 & \dots & \alpha^{n-1} \\ 1 & \alpha^2 & \alpha^4 & \dots & \alpha^{2(n-1)} \\ \vdots & \vdots & \vdots & \ddots & \vdots \\ 1 & \alpha^{n-1} & \alpha^{2(n-1)} & \dots & \alpha^{(n-1)^2} \end{pmatrix}\begin{pmatrix} e^z \\ e^{\alpha z} \\ e^{\alpha^2 z} \\ \vdots \\ e^{\alpha^{n-1}z} \end{pmatrix}, \qquad (A6)$$

which constitutes the matrix form of the discrete Fourier transform [47]. The signal on which this discrete Fourier transform acts contains the function to be symmetrized with arguments shifted by roots of unity.

As shown in the main text, these K functions determine the time evolution at symmetrically splitting EPs of order n. In particular, the asymptotic behavior of the generalized

tangents $T(n, m, z)$ determines the fate of polarizations in these systems.

APPENDIX B: AN EXPLICIT EXAMPLE OF SOLUTION

Here, we give the explicit expression for the evolution operator after one period under the quadratic modulation of Fig. 3(g),

$$
U_f = \begin{pmatrix} D\left(-a - \frac{1}{2}, z_2\right) & D\left(a - \frac{1}{2}, -iz_2\right) \\ iD'\left(-a - \frac{1}{2}, z_2\right) & iD'\left(a - \frac{1}{2}, -iz_2\right) \end{pmatrix}
$$

$$
\times \begin{pmatrix} D\left(-a - \frac{1}{2}, z_1\right) & D\left(a - \frac{1}{2}, -iz_1\right) \\ iD'\left(-a - \frac{1}{2}, z_1\right) & iD'\left(a - \frac{1}{2}, -iz_1\right) \end{pmatrix}^{-1}
$$

$$
\times \begin{pmatrix} D\left(b - \frac{1}{2}, -iy_1\right) & D\left(-b - \frac{1}{2}, -y_1\right) \\ iD'\left(b - \frac{1}{2}, -iy_1\right) & iD'\left(-b - \frac{1}{2}, -y_1\right) \end{pmatrix}
$$

$$
\times \begin{pmatrix} D\left(b - \frac{1}{2}, -iy_0\right) & D\left(-b - \frac{1}{2}, -y_0\right) \\ iD'\left(b - \frac{1}{2}, -iy_0\right) & iD'\left(-b - \frac{1}{2}, -y_0\right) \end{pmatrix}^{-1} \quad \text{(B1)}
$$

where $z_t := 2e^{(i\pi/8)}(t + \frac{i-4}{8})$, $a := -(\frac{7}{64} + \frac{\Delta}{4})e^{(i\pi/4)}$, $y_t := \sqrt{2\sqrt{3}}e^{(i\pi/8)}(t - \frac{i+9}{6})$, $b := -\frac{1+6\Delta}{12\sqrt{3}}e^{(i\pi/4)}$ and $D(\nu, x)$ is the parabolic cylinder function described in Ref. [51].

As described in the main text, the same process can be applied to other modulation curves by solving for each segment independently using the solution to Eq. (34) to construct the operator of Eq. (36) and then concatenating the solutions using Eq. (37). The resulting analytical expression can then be evaluated after one period and diagonalized to obtain the Möbius class. For instance, in the case of a rectangular modulation curve, Eq. (B1) is replaced by a product of eight matrices containing Airy functions, entirely analogous to the case presented here.

[1] M.-A. Miri and A. Alù, Science **363**, eaar7709 (2019).

[2] S. Pancharatnam, Proc. Indian Acad. Sci. **A42**, 86 (1955).

[3] T. Kato, *Perturbation Theory for Linear Operators*, Classics in Mathematics (Springer, Berlin, 1995).

[4] J. Wiersig, S. W. Kim, and M. Hentschel, Phys. Rev. A **78**, 053809 (2008).

[5] W. D. Heiss, Eur. Phys. J. D **60**, 257 (2010).

[6] M. Berry, *A Half-Century of Physical Asymptotics and Other Diversions: Selected Works by Michael Berry* (World Scientific, Singapore, 2017).

[7] H.-Z. Chen, T. Liu, H.-Y. Luan, R.-J. Liu, X.-Y. Wang, X.-F. Zhu, Y.-B. Li, Z.-M. Gu, S.-J. Liang, H. Gao, L. Lu, L. Ge, S. Zhang, J. Zhu, and R.-M. Ma, Nat. Phys. **16**, 571 (2020).

[8] C. M. Bender and S. Boettcher, Phys. Rev. Lett. **80**, 5243 (1998).

[9] A. Mostafazadeh, J. Math. Phys. **43**, 3944 (2002).

[10] A. Mostafazadeh, J. Math. Phys. **43**, 205 (2002).

[11] J. Wiersig, Nat. Commun. **11**, 2454 (2020).

[12] Z. Dong, Z. Li, F. Yang, C.-W. Qiu, and J. S. Ho, Nat. Electron. **2**, 335 (2019).

[13] W. Chen, Ş. K. Özdemir, G. Zhao, J. Wiersig, and L. Yang, Nature (London) **548**, 192 (2017).

[14] Z.-P. Liu, J. Zhang, Ş. K. Özdemir, B. Peng, H. Jing, X.-Y. Lü, C.-W. Li, L. Yang, F. Nori, and Y.-X. Liu, Phys. Rev. Lett. **117**, 110802 (2016).

[15] W. Langbein, Phys. Rev. A **98**, 023805 (2018).

[16] H.-K. Lau and A. A. Clerk, Nat. Commun. **9**, 4320 (2018).

[17] J. Doppler, A. A. Mailybaev, J. Böhm, U. Kuhl, A. Girschik, F. Libisch, T. J. Milburn, P. Rabl, N. Moiseyev, and S. Rotter, Nature (London) **537**, 76 (2016).

[18] A. U. Hassan, B. Zhen, M. Soljacic, M. Khajavikhan, and D. N. Christodoulides, Phys. Rev. Lett. **118**, 093002 (2017).

[19] X.-L. Zhang, S. Wang, B. Hou, and C. T. Chan, Phys. Rev. X **8**, 021066 (2018).

[20] X.-L. Zhang, T. Jiang, and C. T. Chan, Light: Sci. Appl. **8**, 88 (2019).

[21] J. B. Khurgin, Y. Sebbag, E. Edrei, R. Zektzer, K. Shastri, U. Levy, and F. Monticone, Optica **8**, 563 (2021).

[22] T. Needham, in *Visual Complex Analysis* (Oxford University Press, Oxford, 1998), p. 170.

[23] C. Dembowski, B. Dietz, H.-D. Gräf, H. L. Harney, A. Heine, W. D. Heiss, and A. Richter, Phys. Rev. E **69**, 056216 (2004).

[24] A. A. Mailybaev, O. N. Kirillov, and A. P. Seyranian, Phys. Rev. A **72**, 014104 (2005).

[25] R. Uzdin, A. Mailybaev, and N. Moiseyev, J. Phys. A: Math. Theor. **44**, 435302 (2011).

[26] H. Xu, D. Mason, L. Jiang, and J. G. E. Harris, Nature (London) **537**, 80 (2016).

[27] J. W. Yoon, Y. Choi, C. Hahn, G. Kim, S. H. Song, K.-Y. Yang, J. Y. Lee, Y. Kim, C. S. Lee, J. K. Shin, H.-S. Lee, and P. Berini, Nature (London) **562**, 86 (2018).

[28] L. J. Fernández-Alcázar, H. Li, F. Ellis, A. Alú, and T. Kottos, Phys. Rev. Lett. **124**, 133905 (2020).

[29] D. A. Telnov and S.-I. Chu, Phys. Rev. A **71**, 013408 (2005).

[30] S. Longhi and G. Della Valle, Phys. Rev. A **87**, 052116 (2013).

[31] S. Longhi, Europhys. Lett. **117**, 10005 (2017).

[32] T. E. Lee and Y. N. Joglekar, Phys. Rev. A **92**, 042103 (2015).

[33] M. Chitsazi, H. Li, F. M. Ellis, and T. Kottos, Phys. Rev. Lett. **119**, 093901 (2017).

[34] L. Zhou and J. Gong, Phys. Rev. B **98**, 205417 (2018).

[35] J. Li, A. K. Harter, J. Liu, L. de Melo, Y. N. Joglekar, and L. Luo, Nat. Commun. **10**, 855 (2019).

[36] T. T. Koutserimpas and R. Fleury, IEEE Trans. Antennas Propag. **66**, 5300 (2018).

[37] L. Zhou, Y. Gu, and J. Gong, Phys. Rev. B **103**, L041404 (2021).

[38] S. Longhi, J. Phys. A: Math. Theor. **50**, 505201 (2017).

[39] M. V. Berry and R. Uzdin, J. Phys. A: Math. Theor. **44**, 435303 (2011).

[40] H. Deng, Z. Shen, and Q. Xie, Phys. Scr. **94**, 125003 (2019).

[41] J. Gong and Q.-H. Wang, Phys. Rev. A **99**, 012107 (2019).

[42] A. Galda and V. Vinokur, Sci. Rep. **7**, 1168 (2017).

[43] W. Magnus and S. Winkler, *Hill's Equation* (Dover Publications, Mineola, New York, 2004).

[44] H. Mehri-Dehnavi and A. Mostafazadeh, J. Math. Phys. **49**, 082105 (2008).

[45] L. Ge and H. E. Türeci, Phys. Rev. A **88**, 053810 (2013).

[46] D. E. Littlewood, in *A University Algebra* (Heinemann, London, 1950), p. 79.

[47] T. Ceccherini Silberstein, F. Scarabotti, and F. Tolli, in *Harmonic Analysis on Finite Groups* (Cambridge University Press, Cambridge, UK, 2008), Vol. 108, p. 52.

[48] G. W. Hill, Acta Math. **8**, 1 (1886).

[49] E. Mathieu, J. Math. Pure Appl. **13**, 137 (1868).

[50] M. J. O. Strutt, Z. Phys. **69**, 597 (1931).

[51] DLMF, NIST Digital Library of Mathematical Functions, http://dlmf.nist.gov/, Release 1.0.26 of 2020-03-15 (2020), edited by F. W. J. Olver, A. B. O. Daalhuis, D. W. Lozier, B. I. Schneider, R. F. Boisvert, C. W. Clark, B. R. Miller, B. V. Saunders, H. S. Cohl, and M. A. McClain.

[52] G. Floquet, Ann. Sci. Ec. Norm. Sup. **12**, 47 (1883).

[53] A. Liapounoff, in *Annales de la Faculte des Sciences de Toulouse* (Gauthier-Villars, Paris, 1907), Vol. 9, pp. 203–274.

[54] G. Borg, Acta Math. **78**, 1 (1946).

[55] P. Ambichl, K. G. Makris, L. Ge, Y. Chong, A. D. Stone, and S. Rotter, Phys. Rev. X **3**, 041030 (2013).

[56] See Supplemental Material at http://link.aps.org/supplemental/10.1103/PhysRevA.104.042225 for a video of a stability diagram undergoing a transition from real to complex modulation.

[57] F. Minganti, A. Miranowicz, R. W. Chhajlany, and F. Nori, Phys. Rev. A **100**, 062131 (2019).